CHEMISTRY OF MATERIALS

ARTICLE

pubs.acs.org/cm

Insight into the Local Magnetic Environments and Deuteron Mobility in Jarosite ($AFe_3(SO_4)_2(OD,OD_2)_6$, A = K, Na, D_3O) and Hydronium Alunite ($(D_3O)Al_3(SO_4)_2(OD)_6$), from Variable-Temperature ^2H MAS NMR Spectroscopy

Ulla Gro Nielsen,[*,†,‡] Ivo Heinmaa,[§] Ago Samoson,[∥] Juraj Majzlan,[⊥] and Clare P. Grey[*,†,#]

[†]Department of Chemistry and Center for Environmental Molecular Science, State University of New York Stony Brook, Stony Brook, New York 11794-3400, United States

[‡]Department of Physics and Chemistry, University of Southern Denmark, Campusvej 55, 5230 Odense M, Denmark

[§]National Institute of Chemical Physics and Biophysics, Akademia Tee 23, 12618 Tallinn, Estonia

[∥]NMR Instituut, Riia 181A, 51014 Tartu, Estonia; TUT Tehnomeedikum, Akadeemia 1, 12618, Tallinn, Estonia & University of Warwick, Phyics Department, Coventry CV4 7AL, United Kingdom

[⊥]Institute of Geosciences, Friedrich-Schiller University, Burgweg 11, Jena, D-07749, Germany

[#]Chemistry Department, University of Cambridge, Lensfield Rd, CB2 1EW, United Kingdom

ABSTRACT: Detailed insight into the magnetic properties and mobility of the different deuteron species in jarosites ($AFe_3(SO_4)_2(OD)_6$, A = K, Na, D_3O) is obtained from variable-temperature ^2H MAS NMR spectroscopy performed from 40 to 300 K. Fast MAS results in high-resolution spectra above the Néel transition temperature (i.e., in the paramagnetic regime). The ^2H NMR hyperfine shift (δ), measured as a function of temperature, is a very sensitive probe of the local magnetic environment. Two different magnetic environments are observed: (i) Fe_2-OD groups and D_3O^+ ions in stoichiometric regions of the sample. Here, the $\delta(^2H)$ values are proportional to the bulk susceptibility and follow a Curie−Weiss law above 150 K. (ii) Fe-OD_2 groups and D_2O molecules located near the Fe^{3+} vacancies in the structure. The Fe^{3+} ions near these vacancies show strong local antiferromagnetic couplings even high above the Néel temperature (of ca. 65 K). The D_2O and D_3O^+ ions located on the jarosite A site can be distinguished in the ^2H NMR spectra due to the different temperature dependence of their isotropic shifts. Motion of the D_3O^+ ions was followed by investigating the isostructural (diamagnetic) compound $(D_3O)Al_3(SO_4)_2(OD)_6$ and an activation energy of 6.3(4) kJ/mol is determined for the D_3O^+ motion. Our NMR results support theories that ascribe the spin glass behavior that is observed for $(H_3O)Fe_3(SO_4)_2(OD)_6$ but not for the other cation substituted jarosites, to the disorder of the D_3O^+ ions and/or a less distorted Fe coordination environment. No signs of proton transfer reactions from the D_3O^+ ion to the framework are observed.

KEYWORDS: jarosite, paramagnetism, spin-glass, solid-state NMR, iron sulfate, Kagomé, ^2H NMR, proton dynamics

INTRODUCTION

Jarosites, $AFe_3(SO_4)_2(OH)_6$, (A = Na, K, Rb, H_3O, NH_4, Ag, Pb(II), ...), are mixed-metal iron(III) sulfates that have attracted interest from a wide area of sciences including geochemistry, terrestrial and Martian geology, metallurgy, and materials science.[1,2] The naturally occurring jarosite minerals (e.g., A = Na, K, H_3O, Pb(II)) are often associated with acid mine drainage[3] because they are formed under aqueous, acidic conditions. The identification of jarosite in the Mössbauer spectra of Martian rock received much attention as it was interpreted as evidence for the presence of water in the prehistory of Mars.[4−6] In materials science, the magnetic properties of jarosite and the isostructural V(III)[7−9] and Cr(III)[10] analogues have been extensively studied because they are examples of frustrated magnetic systems,[11−14] their magnetic responses depending noticeably on the nature of the cations and on the presence of disorder.[15−34]

Local Structure in Jarosite and Alunite. Jarosite and alunite are the isostructural end members of the alunite group of minerals crystallizing in the $R\bar{3}m$ space group.[1] Figure 1 shows their crystal structure, which consists of layers of octahedrally coordinated Fe(III) or Al(III) ions at the nodes of a so-called 2D Kagomé lattice. For jarosite, the layers comprise Fe(III) ions located on the corners of an equilateral triangle with Fe−Fe distances of 3.65 Å,[33] where the Fe−Fe distance is independent of the nature of the A cation, this trimer forming the magnetic subunit (Figure 1). The shortest interlayer Fe−Fe distance is ca. 6 Å.[33] The structure of the Kagomé layer is to a first approximation insensitive to cation substitution, whereas the interlayer spacing (and *c*-axis) is directly related to the size of the cation.[1] The Kagomé layers are connected through H-bonding involving the equatorial Fe_2-OH group and the apical oxygen in the sulfate group above, i.e., ($Fe_2-O-H-O{=}S$) with a O−H−O distance of ca. 2.88 Å.[23]

Jarosite is a text book example of a 2D Kagomé lattice,[11,33] antiferromagnetic coupling of the three iron(III) ions in the magnetic subunit (trimer), leading to geometrical frustration.[11,13]

Received: February 7, 2011
Revised: May 14, 2011
Published: June 09, 2011

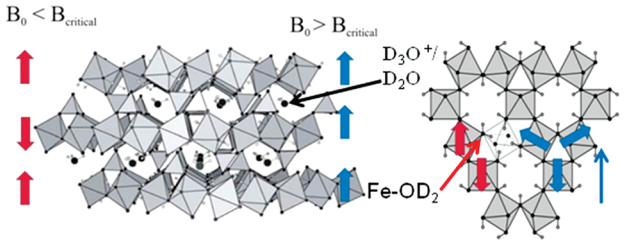

Figure 1. Structure of jarosite viewed along the *a*-axis (left) illustrating the layered structure of jarosite. The arrows illustrate the magnetic coupling between the individual Kagomé layers for magnetic field strengths (B_0) above and below the critical magnetic field ($B_{critical}$). The three blue arrows show the magnetic subunit in the Kagomé lattice (right), which is frustrated. Introducing a Fe vacancy lifts the frustration and allows the two adjacent Fe ions to couple antiferromagnetically (red arrows). The charge compensation mechanism for vacancies is described in eq 1.

To a first approximation, this intralayer antiferromagnetic coupling is the dominant interaction and as a result, a Néel transition temperature (T_N) at ca. 65 K is observed for all jarosites, except for hydronium jarosite (A = H_3O), irrespective of the *A* site cation.[17,26,35] Although jarosites are paramagnetic above T_N, Nocera et al. observing that their susceptibility obeys a Curie–Weiss (CW) law above 150 K,[7] Harris et al. modeled the susceptibility data with a CW law scaled by a factor of 8/9 in the low-temperature regime (below ca. 350 K),[26] because of the geometry of the Kagomé lattice and the high frustration of the magnetic lattice (the Weiss constant, $\Theta \gg T_N$).[17,18,26]

Jarosites are notorious for the presence of up to 30% Fe(III) vacancies, and substantial numbers of A site vacancies.[11,36] Because the introduction of a Fe^{3+} vacancy in the triangular magnetic unit removes the frustration and allows the two remaining iron spins to couple (anti)ferromagnetically, as illustrated in Figure 1, the long-range (magnetic) order (LRO), that is observed in many synthetic and natural samples, was originally ascribed to these Fe(III) vacancies.[25,26] However, LRO was later observed in stoichiometric jarosites,[17,30,35,37] ruling out defects as the origin of LRO. Theoretical calculations originally ascribed the cause of the LRO to second-order crystal field effects caused by deviations from octahedral symmetry of the $FeO_2(OH)_4$ octahedra, which lift the degeneracy of the t_{2g} and e_g orbitals.[24] Theoretical calculations showed that the Dzyaloshinsky–Moriya (DM) interaction ($H_{ij} = \boldsymbol{D}(\boldsymbol{S}_i \times \boldsymbol{S}_j)$) in jarosite is allowed because of the geometry of the kagomé lattice.[12] The absence of an inversion center between each Fe pair and the tilting of the FeO_6 octahedron allows for a canting of the individual magnetic moments out of the Kagomé plane thereby producing a net magnetic moment perpendicular to this plane.[12,14,15,22,37] Theoretical calculations have predicted that the DM interaction is larger than the crystal field effects,[12,14] a prediction that has subsequently been verified experimentally.[7,14,22,28,30] The interlayer interaction is antiferromagnetic resulting in a magnetic unit cell, that is twice that of the crystallographic unit cell.[10,20,26,32] Placing the sample in a magnetic field of 14 kOe (1.4 T) or higher forces a change in the interlayer interactions and ferromagnetic ordering of the net moment is observed,[15,37] a phenomenon that may be important in the NMR studies described below.

Hydronium jarosite does not, unlike the other jarosites, exhibit antiferromagnetic ordering, but is instead a spin-glass with a glass transition temperature at ca. 17 K.[21,36] Originally this was ascribed to the fact that the hydronium jarosites were almost completely stoichiometric and could not order antiferromagnetically, but this is counter to the observation of spin-glass behavior in recent thermodynamic studies of defect containing K–H_3O jarosites by Majzlan et al.[27] Currently, the presence of the hydronium ion is thought to be important in causing the spin glass behavior. Wills and Harrison suggested a structural disorder of the hydronium ion over the different sites in the jarosite cavities (where the crystallographic H site occupied by the H_3O^+ ion is half filled).[36] In contrast, Grohol et al.[16,17] proposed an internal acid–base reaction between the hydronium ion and the μ-Fe_2–OH group so that H_2O molecules are found in the cavities, i.e.

$$Fe_2{-}OH + H_3O^+ \rightarrow Fe_2{-}OH_2^+ + H_2O \qquad (1)$$

Our recent solid-state NMR(SSNMR) investigations of deuterated jarosite and its isostructural aluminum analogues did not find any evidence for chemical exchange between D_3O^+ and Fe/Al_2–OD groups.[23,38] Distinct resonances were observed which could be assigned to FeO(D)–Fe, Fe–OD_2, and D_3O^+/D_2O local environments, the Fe–OD_2 resonance being absent in stoichiometric samples. We also proposed a new mechanism for charge compensation of the vacancy, involving the hydronium ion on the A site and the four adjacent terminal Fe/Al (M^{3+})-O^{2-} groups on the B site, created by the vacancy, resulting in a neutral water molecule. Formally, we can write the reaction for the removal of an M^{3+} ion from its local coordination environment $(M(OH)_4O_2)^{5-}$ to form a vacancy □ as follows, where the bridging –O(H)– groups have been replaced by terminal $-OH_2$ groups:

$$M(OH)_4O_2^{5-} + 3H^+ + H_3O^+ \rightarrow \square(OH_2)_4O_2^{4-} + H_2O + M^{3+} \qquad (2)$$

^{2}H static NMR spectroscopy has previously been reported for a series of defective deuterated alunite samples by Ripmeester et al. from room temperature down to 77 K.[39] Their spectra showed a gradual freezing of the D_3O^+ ion between 150 and 77 K consistent with the absence of a well-defined energy barrier and a broad range of activation energies, E_a of 12–17 kJ/mol was reported. Mashiyama et al. investigated jarosites down to 1.76 K by wide line ^{1}H static NMR and identified the presence of a single ^{1}H environment in the antiferromagnetic phase.[24] Here we present a variable temperature (VT) ^{2}H MAS NMR study of a series of jarosite and of an isostructural hydronium alunite, which gives detailed insight into the mobility of the different deuteron species and the local magnetic properties nearby these species. The use of fast magic-angle spinning (40 kHz), which is a challenge at such low temperatures, results in superior spectral resolution as compared to the earlier static NMR studies.[24,39] Both stoichiometric and defect jarosite samples are investigated along with a near-stoichiometric hydronium alunite. The current study gives a unique view of how structural defects affect the local magnetic properties in various jarosite samples.

EXPERIMENTAL SECTION

Samples. A detailed description of the syntheses and characterization of the jarosite samples by powder X-ray diffraction (XRD) and ^{2}H MAS NMR at ambient temperature has recently been reported.[23] The four jarosite samples investigated by variable (VT) temperature ^{2}H NMR are (i) a stoichiometric jarosite with A = K (Stoic-jaro) prepared using the method of Grohol et al.[17] with metallic iron and (ii) three

dx.doi.org/10.1021/cm2003929 |*Chem. Mater.* 2011, 23, 3176–3187

Table 1. ^{2}H Quadrupole Coupling Parameters and Dipole Couplings for the Different Local Environments in the Jarosite Samples Estimated Based on the Method of Siminovitch et al.[66] ^{2}H NMR Parameters for D_3O-alu are Given for Comparison[38]

sample	resonance	δ (ppm)	C_Q (kHz)	η_Q	$d_{electron}$ (ppm)	intensity (%)[a]
Stoic-jaro	Fe_2−OD	237(4)	220(8)	≈ 0	912(260)	100
D_3O-jaro	Fe_2−OD	240(60)	233(15)	≈ 0	1173(500)	57(33)
	Fe-OD_2	70(30)	114(15)	≈ 1	293(500)	14(14)
	D_nO	0(10)	98(15)		0(500)	29(2)
K-jaro	Fe_2−OD	240(60)	245(15)	≈ 0	890(500)	63(5)
	Fe-OD_2	130(30)	99(15)	≈ 1	0(500)	29(4)
	D_nO	5(10)[b]	98(15)		0(500)	8(2)
Na-jaro	Fe_2−OD	230 (60)	227(15)	≈ 0	1000(500)	68(5)
	Fe-OD_2	64(30),	99(15)	≈ 1	98(500)	16(3)
	D_nO[c]	1(10)	99(15)		0(500)	16(3)
D_3O-alu	Al_2−OD	4.0(5)	235(9)	0.0	N/A	N/A
	D_3O^+	10.1(5)	17(5)	≈ 0.45	N/A	N/A

[a] The spectral intensities were obtained from integration of ^{2}H MAS NMR spectra recorded at a 35 kHz spinning speed spectra and are normalized to 1. [b] Two partly resolved peaks at ca. 0.5 and 9.7 ppm. [c] D_2O and D_3O^+ resonances overlap at room temperature (see text).

nonstoichiometric jarosite samples with A = Na, K, and D_3O^+, respectively using conventional hydrothermal synthesis with hydrous Fe(III) sulfate as the iron source.[23] The latter are labeled according to the convention A-jaro, i.e., K-jaro, Na-jaro, and D_3O-jaro. In addition, an isostructural stoichiometric (within the experimental uncertainty) deuteronium alunite ($(D_3O)Al_3(SO_4)_2(OD)_6$, D_3O-alu) was investigated. Synthesis and characterization of this sample by XRD and room temperature ^{1}H, ^{2}H, and ^{27}Al NMR have been reported elsewhere.[38]

NMR. ^{2}H MAS NMR experiments employed a single-channel 1.8 mm MAS probe tuned to ^{2}H and encapsulated in a low temperature cryostat from Janis Research Co., Wilmington, MA. Experiments were performed on a 360 MHz (8.4 T, $\nu_L(^2H)$ = 55.2 MHz) Bruker NMR spectrometer for Stoic-jaro, K-jaro, Na-jaro, and D_3O-alu. ^{2}H NMR experiments for D_3O-jaro were performed on a 200 MHz (4.7 T, $\nu_L(^2H)$ = 30.7 MHz) Bruker NMR spectrometer. Spectra were recorded by using a Hahn-echo with one or two rotor periods, to alleviate problems with spectrometer dead time and probe ringing, and spinning speeds in the range 15 − 42 kHz. The longitudinal (spin−lattice) relaxation (T_1) was measured at selected temperatures for Stoic-jaro, K-jaro, D_3O-jaro, and D_3O-alu using the inversion recovery experiment followed by a rotor-synchronized Hahn-echo (180°− t_1−90$_x$°−τ−180$_x$°−τ−acq; $\tau = 2t_r$) again to alleviate problems with the probe ringing. The inversion recovery data were analyzed using the Bruker software on the spectrometer. The T_2^*, $(T_2^*)^{-1} = (T_2)^{-1} + (\gamma\Delta B_o)/2$, where T_2 is the true transverse relaxtion time and T_2^* is the effective T_2, which includes the contribution due to magnetic field inhomogeneities and distributions in chemical/hyperfine shifts, was determined from deconvolution of the isotropic peak using DMFit.[40]

Experiments were performed from 300 K down to ca. 40 K and the temperature regulated by heating the helium gas using a temperature controller from Lakeshore Cryotronics Inc. Model 240. Helium gas was used for spinning. Typically, the temperature varied 1−3 K during the course of an experiment. The temperature difference between the readout temperature on the sensor and actual temperature of the rotating sample did not exceed 5 K.[41−43]

A liquid sample of D_2O was used for referencing ($\delta_{iso}(^2H)$ = 4.8 ppm) and r.f. calibrations. The r.f. efficiency is temperature dependent. Thus, pulses lengths were adjusted when spectral artifacts due to imperfect pulses were observed. Magic angle setting was done at room temperature by minimizing the line width of the spinning sideband (ssbs) in a ^{23}Na MAS NMR spectrum of $NaNO_3$. No significant deviations from the magic angle were observed during the course of a VT experiment, as observed from the line widths of D_3O-alu. The magnetic field inside the cryostat is dependent on temperature. This results in a negative shift of ca. −14 ppm at 50 K, −6 ppm at 100 K, and negligible (<2 ppm) above 120 K.

Table 2. Magnetic Data Extracted from Analysis of $\delta^{-1}(T)$ for Stoic-jaro, K-jaro, Na-jaro, and D_3O-jaro in the Region Where a Linear Relationship Is Observed (Figure 10)[a]

aample	δ_{0K} (ppm)	Θ (K)	temperature range (K)
Stoic-jaro; Fe_2−OD	304(20)	−1110(100)	150−300
K-jaro, Fe_2−OD	301(20)	−986(100)	141−300
Na-jaro, Fe_2−OD	296(20)	−901(100)	151−300
D_3O-jaro, D_3O^+	173(200)	68(40)	69−300
D_3O^+	25(200)	30(40)	104−300

[a] The temperature range listed here corresponds to the range used to fit the data to the Curie-Weiss law in Figure 10.

RESULTS AND DISCUSSION

The results for the deuterated alunite sample D_3O-alu are presented first, as investigations of the diamagnetic D_3O-alu allow studies of the molecular motion to be performed in the absence of magnetic effects, the latter simplifying the spectra and increasing spectral resolution. Here our focus is to probe the mobility of the hydronium ion, as this may give insight into the spin glass properties of the isostructural hydronium jarosite. This is followed by the results for Stoic-jaro, and then the more complex nonstoichiometric samples (K-jaro, Na-jaro, and D_3O-jaro). Table 1 summarizes the ^{2}H NMR data obtained from all the ambient temperature studies.[23,38] A detailed joint analyses of the ^{2}H NMR data in the CW regime is given at the end of the section for all four jarosite samples. These results are summarized in Table 2.

D_3O-alu. The deuteronium alunite (D_3O-alu) investigated here has near full occupancy (>98%) of the Al sites and a high concentration of hydronium ions on the *A* site, as evident from the SSNMR and elemental analysis.[38] ^{1}H and ^{2}H MAS NMR unambiguously shows the presence of hydronium ions in this sample.[38,39] The ^{2}H MAS NMR spectrum contains two sets of spinning sideband (ssbs) manifolds, which are assigned to the Al_2−OD group and a D_3O^+ ion.[38] The first corresponds to species that are hydrogen bonded and rigid, and the latter to species that are highly mobile at room temperature.[38] ^{2}H MAS NMR spectra were recorded in this study in a temperature range from 40 to 300 K (Figure 2) and were analyzed by visual inspection and by determining the T_1 times (Figure 3a) at selected temperatures. The motion of the hydronium ions slows down at around 150 K and freezes on the NMR time scale at 125(10) K. Below this temperature, the characteristic line shape (Pake doublet) of a rigid, hydrogen bonded O−D−O group is observed. We note that the fast, unregulated spinning speeds ($\omega_r/2\pi \approx 20$ kHz; 10−50 Hz variation during an experiment), and the limited number of scans used to acquire the spectra, combined with a narrow probe bandwidth, do not allow accurate determination of the ^{2}H quadrupole coupling from analysis of the ssb intensities. The changes in motion are also reflected by

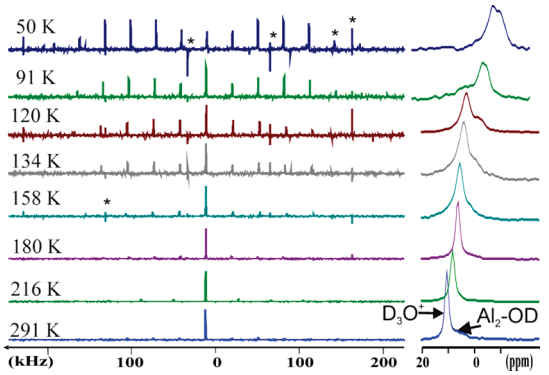

Figure 2. Selected ^{2}H MAS NMR spectra of D_3O-alu recorded in the temperature range 50−291 K. Spectra were recorded using spinning speeds of 15−20 kHz using an echo sequence. The asterisks mark "spikes" that are artifacts arising caused by the electronic circuit. The apparent temperature dependence of δ_{iso} is caused by a temperature dependent shift from the cryostat. This shift is ca. −10 ppm at 50 K, but negligible above ca. 100 K.

the T_1 times, (Figure 3). The T_1 times were extracted by fitting the data to a single exponential. Again, only the isotropic resonance was used in this analysis due to the fluctuations in the spinning speed. The spin−lattice relaxation of a $I = 1$ nucleus is not always best described by a single exponential[44] since the T_1 for ^{2}H is anisotropic, the quadrupolar coupling depending on the orientation of the crystallites with respect to the magnetic field.[45] However, a good fit to the data was obtained, given the fairly large uncertainty in the determination of T_1, so a more complex analysis of the data could not be justified. The plot of T_1 as a function of temperature exhibits a T_1 minimum at 125 K. This minimum occurs when the correlation time for motion, τ_c, is approximately equal to the Larmor frequency (55 MHz) corresponding to $\tau_c \approx 18$ ns. If the molecular motion has a well-defined activation energy, E_a, the correlation time shows an Arrhenius behavior.[46]

$$\tau_c = \tau_\infty \exp\left(\frac{E_a}{k_B T}\right) \quad (3)$$

where τ_∞ is the correlation time at infinite temperature. Thus, by plotting $\ln(1/T_1)$ as a function of the inverse temperature, E_a can be determined.[46]

$$\ln(1/T_1) \propto \frac{E_a}{k_B}\frac{1}{T} \quad (4)$$

$E_a = 6.3(4)$ kJ/mol ($r^2 = 0.99$) is obtained for D_3O^+ motion using data points above the T_1 minimum. The low temperature part of the curve is not linear, as is apparent from Figure 3b. The sharp, well-defined T_1 minimum does however indicate a well-defined energy barrier for the deuteronium ion's motion.

Our results deviate somewhat from those of Ripmeester et al. obtained for similar materials.[39] Their use of static ^{2}H NMR resulted in an overlap of the resonances, which was particularly severe for the Al-OD_2 and D_2O/D_3O^+ resonances as they both have quite similar quadrupole coupling constants.[39] In addition, they were unable to unambiguously determine whether D_2O or D_3O^+ were present, this requiring ^{1}H MAS NMR.[39] They observed that the deuteron motion slowed down around 160 K and at 90 K, a Pake doublet was observed. These authors estimated an activation energy barrier of 12−17

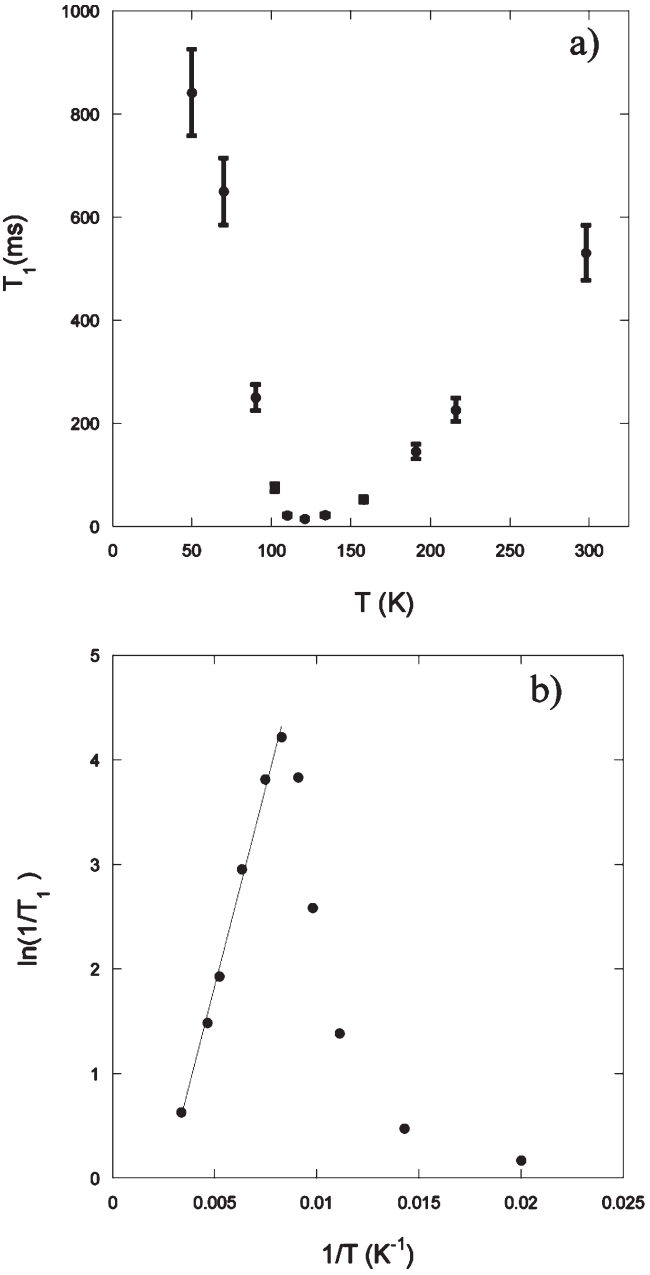

Figure 3. (a) T_1 for the isotropic peak of the D_3O^+ groups of D_3O-alu as a function of temperature, T (K) and (b) $\ln(1/T_1)$ as a function of T^{-1}. Linear regression was used for determination of E_a.

kJ/mol based on the temperature range in which the motion stopped, the results implying the absence of one well-defined energy barrier.[39] We suggest that the analysis of T_1 data along with the ability to resolve the different species most likely represents a more accurate method for probing deuterium motion than the analysis of overlapping ^{2}H static line shapes, but it may also be that some of the discrepancies between the two sets of results arise from differences in the samples. Recent first principles MD simulations have investigated the structure and mobility of the H_3O^+ ion in alunite.[66] These results showed a rapid reorientation of the H_3O^+ between sites involving hydrogen bonding to the Fe_2OH and sulfate oxygen atoms, and the occasional umbrella inversion, on the ps time scale. This is rapid

dx.doi.org/10.1021/cm2003929 |Chem. Mater. 2011, 23, 3176–3187

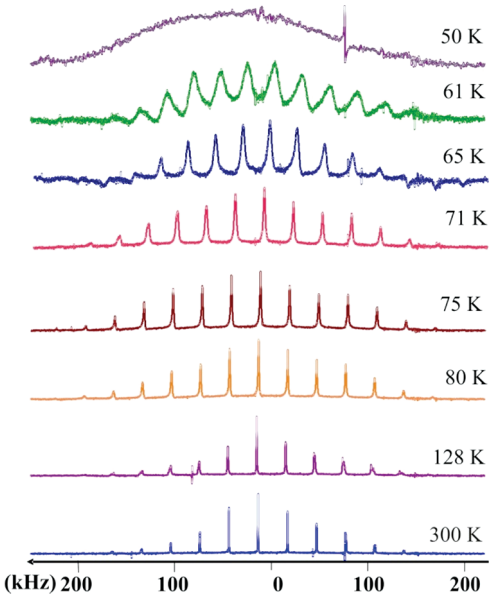

Figure 4. ^{2}H NMR spectra of Stoic-jaro from 50 to 300 K recorded at 55.6 MHz and with an ~30 kHz spinning speed. The sample temperature is listed next to the spectrum.

motion is consistent with the low activation energy derived from our T_1 analysis.

Stoic-jaro. This sample was prepared following a reported procedure to synthesize stoichiometric jarosite[17] and is indeed stoichiometric according to our previous ^{2}H NMR and electron microprobe analysis.[38] Room temperature ^{2}H MAS NMR spectra show the presence of a single ^{2}H site characterized by δ = 237(4) ppm, C_Q = 220(8) kHz, and $\eta_Q \approx 0$, which is assigned to a Fe−O(D)−Fe deuteron.[23] The asymmetry in the spinning sideband manifold is caused by the electron−nuclei dipolar interaction, estimated to be approximately $d_{electron}$ = 912(260) ppm, ($d_{electron} = d_{zz} - \delta$).[23] Figure 4 shows the change in the overall appearance of the ^{2}H MAS NMR spectra upon cooling from room temperature to 50 K, where the spectral resolution is lost. The most significant changes are observed for the position of the isotropic resonance and the line width of the individual ssbs (Figures 4, 5a, and 6). The isotropic resonance is located at 237(4) ppm at 300 K and slowly reaches a maximum of 269(1) ppm over a wide temperature range between 145 and 115 K; it then rapidly drops to ca. −60 ppm at 61 K, as illustrated in Figure 5a. At 50 K, i.e., below T_N, the spectrum consists of a broad featureless resonance 3−400 kHz in width and no individual ssbs can be resolved (Figure 4). No other ^{2}H resonances are observed in the entire temperature range from 50 to 300 K, confirming that the sample is stoichiometric, i.e., Fe−OD_2, D_2O, and D_3O^+ are not present in the sample. It is well-known that molecular motion on the NMR time scale can result in disappearance of resonances, however, it is unlikely that the resonances are invisible over a 250 K temperature range (see discussion for K-jaro vide infra). These results are consistent with a field-swept ^{1}H study of NMR of jarosite,[47] which showed the presence of a single H site.

The relaxation rate (T_1) measured for the Fe−O(D)−Fe deuteron changes from 25.5(2) ms at room temperature to 14(1) ms at 64 K. This is accompanied by a noticeable increase in the line width from 0.5 to 5 kHz, as illustrated in Figure 6. For comparison, the line width for D_3O-alu remains approximately constant at only 250(50) Hz over the same temperature range. Thus, the line width is mainly dictated by the ^{2}H relaxation (T_2) rate and not by a distribution of the paramagnetic shifts caused by local structural variations for this stoichiometric sample. However, $T_2^* < T_1$ and it is likely that the short T_2 values are caused by both the ^{2}H motion and the fluctuating electronic moments, the latter slowing down considerably as the sample approaches T_N.

K-jaro. This is a defect jarosite (A = K) sample with 30% K^+ and 10% Fe vacancies.[23] A composition of $[K_{0.70(9)}(D_3O)_{0.01(8)}(D_2O)_{0.30(8))}]_A[Fe_{2.7(1)}(OD)_{4.8(2)}(OD_2)_{1.2(2)}]_B(SO_4)_2$ was previously evaluated from the ^{2}H NMR and electron microprobe analysis, the parentheses indicating the cations on the A site and B site/framework, the OD_2 groups on the B site/framework referring to the Fe-OD_2 groups created by the presence of a vacancy and reaction (2). Very little (essentially no) hydronium on the *A* site is present. Three different local environments are observed in the ^{2}H MAS NMR spectra recorded at room temperature: a rigid Fe_2−OD (δ = 240(60) ppm), a Fe-OD_2 group rotating around the Fe−O bond vector (δ = 70(30) ppm) and a mobile, D_2O molecule on the A site with (δ = 5(10) ppm), as discussed in detail in ref.[20] The Fe_2−OD and Fe-OD_2 resonances are quite broad due to a distribution in hyperfine shifts caused by both variations in the local magnetic moments[48] and local structures, arising from the presence of ca. 10% Fe vacancies in the structure.[23] Each Fe has four Fe(III) ions in the first cation (Fe) coordination sphere (Figure 1). Thus, approximately 35% of all Fe ions in the Kagomé lattice have one or more vacancies as nearest neighbors assuming a random distribution of the 10% of Fe^{3+} vacancies in the Fe(III) layer, and will thus be present as terminal Fe-OD_2 groups. The temperature dependence of the framework Fe_2−OD isotropic resonance is similar to that observed for the Fe_2−OD group in stoic-jaro: A comparison of Figure 5a,b shows that the isotropic shift of the Fe_2−OD groups in both compounds reaches a maximum at around 120 K and then rapidly decreases as the temperature is lowered further. However, at 71 K, just above T_N, a value of 210(30) ppm is observed whereas the corresponding value for stoic-jaro is 177 ppm at this temperature. We assign this difference to the presence of Fe(III) vacancies located in more distant coordination shells of the Fe_2−OD groups, which will affect the local magnetic interactions.

Rapid rotation of the OD_2 group around the Fe−O bond vector for the Fe−OD_2 group results in a partial averaging[49] of the ^{2}H quadrupole coupling to 70 kHz at room temperature. This motion gradually slows down as the temperature is lowered and freezes on the ^{2}H NMR time scale ($\approx \mu$s) between 140 and 120 K (Figure 7). In contrast to the Fe_2−OD group, the hyperfine shift for the Fe−OD_2 group remains fairly constant between 40 and 60 ppm over 250 K (from 60 to 300 K) (Figure 5b), implying the presence of strong local antiferromagnetic couplings presumably caused by the presence of a Fe vacancy next to the Fe−OD_2 group: vacancies remove the frustration and allow for local antiferromagnetic coupling between the two remaining iron(III) ions in the magnetic subunit, as illustrated in Figure 1. We have also observed strong local antiferromagnetic interactions for ^{2}H in pristine iron oxyhydroxides (α- and β-FeOOH), which resulted in a similar lack of temperature dependence of the NMR hyperfine shift just above T_N.[50,51]

The D_2O molecule on the A site gives rise to a single resonance with a line shape that is consistent with rapid, near-isotropic molecular motion at room temperature. The resonance splits in two in spectra recorded at 191 K and below (Figures 5b

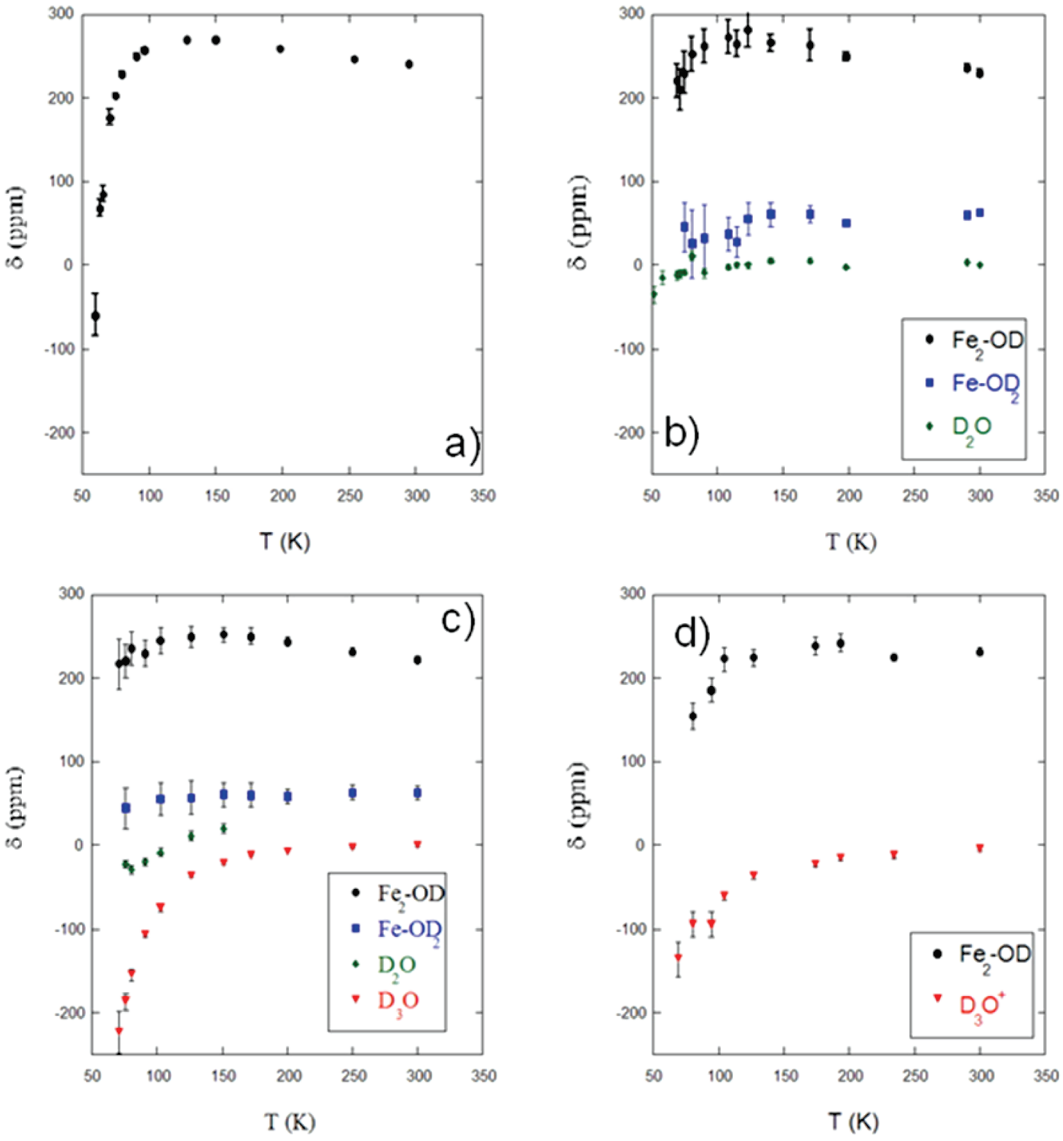

Figure 5. ^{2}H isotropic shift, δ, as a function of temperature for (a) Stoic-jaro (Fe_2—OD only), (b) K-jaro, (c) Na-jaro, and (d) D_3O-jaro. The isotropic peak was defined as the center of gravity for each resonance and the uncertainty reflects the estimated uncertainty in determining the actual position. This is most difficult for the Fe-OD_2 resonance as this is the broadest peak, of lowest intensity and is sandwiched between the Fe_2—OD and D_nO resonances. The D_nO resonance is fairly narrow, and therefore it is possible to determine the isotropic peak more precisely.

and 7), the lower field resonance accounting for 90% of the intensity (marked by "1" in the 121 K spectrum in Figure 7). Only the most intense peak is plotted in Figure 5. The intensity of the D_2O resonances decreases upon cooling reaching a minimum between 120 and 140 K, as the molecular motion enters the time scale of the rotor echo spacing (ca. 60 μs). Intensity is restored upon further cooling (Figure 7) and below 120 K, the ssb pattern is characteristic of that of a rigid D_2O molecule is seen.

Measurements of T_1 relaxation were performed at selected temperatures between room temp and 99 K (not shown). The T_1 time for Fe_2—OD remains constant at ≈20(5) ms over the entire temperature range unlike the T_1 of for the Fe_2—OD group in stoic-jaro (vide supra). In summary, SSNMR shows that K-jaro is a defect jarosite with two different local magnetic environments, (i) stoichiometric regions with a temperature dependence of $\delta(^2H)$ similar to that observed for stoic-jaro and (ii) defect regions with Fe vacancy nearby, where strong local antiferromagnetic interactions result in nearly temperature-independent isotropic shifts for the Fe-OD_2 groups and D_2O ions on the A site.

Na-jaro. The composition of this sample is $[Na_{0.53(9)}(D_3O)_{0.31(8)}(D_2O)_{0.16(4)}]_A[Fe_{2.85(5}(OD)_{5.4(2)}(OD_2)_{0.6(2)}]_B(SO_4)_2$ based on our earlier ^{2}H NMR measurements and elemental analysis[23] and a significant concentration of both D_2O and D_3O^+ appear to be present in this sample. Analysis of the variable temperature NMR (Figure 8) shows that the temperature dependence of the isotropic shift for the Fe_2—OD and Fe-OD_2 groups resembles that observed for K-jaro c.f., Figures 5b and c. Thus, $\delta(Fe_2$—OD) follows a CW law above 150 K, whereas δ(Fe-OD_2) is nearly independent of temperature down to T_N (Figure 5c). The isotropic resonance for the D_nO group does not vary by more than ca. 10 ppm from RT down to 150 K as observed for K-jaro (vide supra). At 150 K the resonance splits into two resonances with very different

dx.doi.org/10.1021/cm2003929 |*Chem. Mater.* 2011, 23, 3176–3187

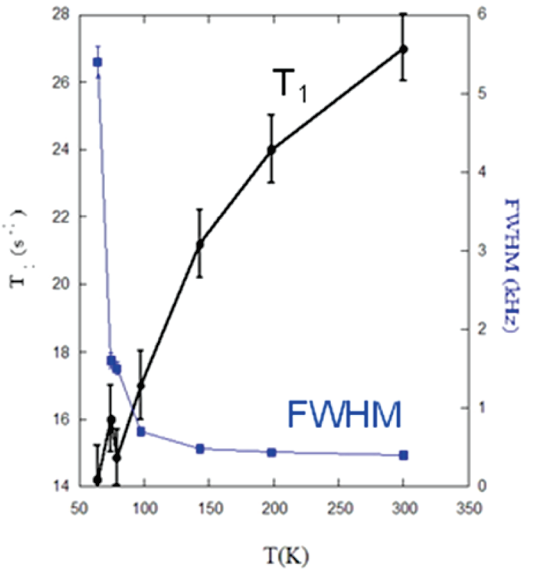

Figure 6. T_2 and the line width (full width, half-maximum; fwhm) for the isotropic resonance for stoic-jaro plotted as a function of temperature.

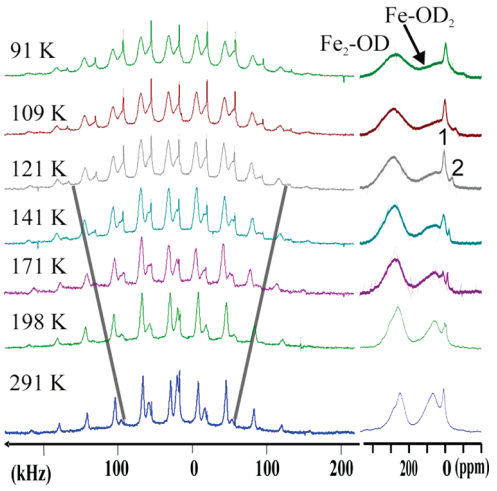

Figure 7. ^{2}H MAS NMR spectrum of K-jaro in the temperature range from 91 to 291 K; spinning speeds of about 40 kHz were employed. The two lines show the position of the outermost (readily detected) ssb for the Fe-OD_2 group and illustrate how the motion of this group slows down. To the right is an expansion of the isotropic shift region. The D_nO peaks split into two peaks below 198 K, labeled as 1 and 2 in the 121 K spectrum.

temperature dependences of the isotropic shift, as is evident in Figure 5c: the most intense resonance rapidly becomes more negative as the Néel temperature is approached whereas the weaker resonance does not change significantly. By analogy with K-jaro, the weaker resonance is assigned to D_2O located near a Fe vacancy, i.e., in a magnetic environment characterized by strong local antiferromagnetic interactions. The most intense peak has a temperature dependence similar to that observed for the D_3O^+ ion in D_3O-jaro (vide infra) and is assigned to D_3O^+ located in stoichiometric regions of the sample.[23] A relative intensity of approximately 1:3 for D_2O:D_3O^+ is expected based on stoichiometry. However, the observed D_2O intensity is much smaller than this, which most likely is due to a combination of *i)* the D_2O

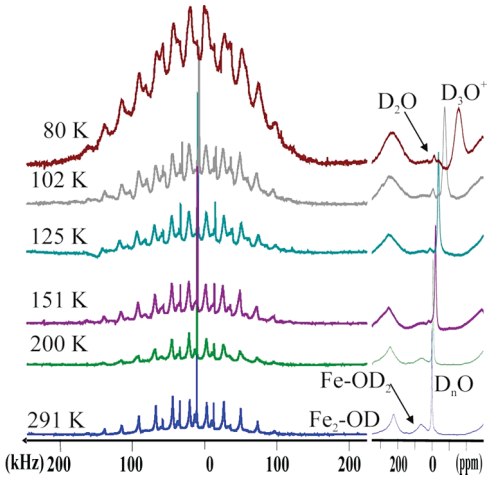

Figure 8. ^{2}H MAS NMR spectrum of Na-jaro in the temperature range 80−291 K; spinning speeds of about 40 kHz were employed. An expansion of the isotropic region is illustrated to the right.

motion is on the time scale of the Larmor frequency between 190 and 120 K, which results in a loss of signal intensity (we observe that the D_2O intensity is similarly weaker in K-jaro in this temperature range due to motion c.f., Figure 7) and (ii) the presence of less D_2O in the structure, e.g., due to exchange with H_2O over time or dehydration, resulting in vacancies on the A site, as the neutral water molecule is not needed for charge balance.[23,38] The results for Na-jaro clearly illustrate the strength of solid-state MAS NMR as a tool for probing local properties in complex paramagnetic materials, where multiple local environments with different magnetic properties are present. This behavior would be very difficult to probe with susceptibility measurements (bulk technique) or diffraction studies.

D_3O-jaro. This sample has a composition $[(D_3O)_{0.84(3)}(D_2O)_{0.09(20)}]_A[Fe_{2.84(3)}(OD)_{5.4(1)}(OD_2)_{0.6(1)}]_B(SO_4)_2$ based on our previous ^{2}H NMR and elemental analysis.[38] The low temperature phase of hydronium jarosite is, unlike the other jarosites, a spin-glass with a spin-glass transition temperature at ca. 17 K.[17,21] From room temperature to about 100 K, the isotropic resonance from the highly mobile D_3O^+ ion dominates the spectra (Figure 9), and only a weak ssb on each side of the isotropic resonance observed. This reflects rapid motion and almost complete averaging of the ^{2}H quadrupole coupling, as is also observed for D_3O-alu. Upon cooling, the intensity of the isotropic resonance decreases, while the intensity of the ssbs increase and additional ssbs appear indicating a slowing down of the rapid motion. At 90 K the innermost ssbs have approximately one-third the intensity of the central transition and the D_3O^+ ion motion has slowed down significantly. However, the ssb pattern for the D_3O^+ group even at low temperature does not look like the classic Pake doublet observed for the ion in D_3O-alu (vide infra). This is ascribed to the following phenomena: (a) the D_3O-jaro sample was investigated by ^{2}H MAS NMR at 30.7 MHz, where the Q-factor for the probe was high,[52] which combined with fast MAS (20−40 kHz) resulted in most of the intensity being distributed in the center band. The other samples were studied at 55 MHz and did not suffer from these experimental issues. (b) Interactions with the unpaired electrons that distort the line shape, the distribution of interactions in the spin glass complicating the analysis further. (c) A distribution in correlation times for motion may be present, the more mobile D_3O^+ ions with larger residual

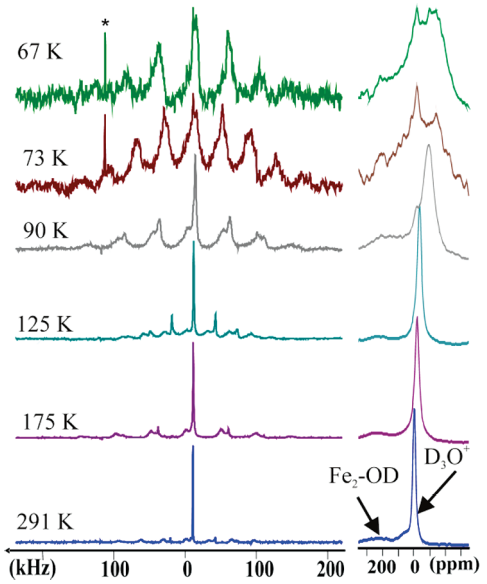

Figure 9. ^{2}H MAS NMR spectra of D_3O-jaro from 50 to 291 K recorded with a spinning speed of approximately 40 kHz. The samples temperature is indicated on each spectrum. The resonance indicated with an asterisk is an electronic artifact. An expansion of the isotropic region is shown to the right. Note that the D_3O^+ ion resonance dominates at high temperatures. The weak Fe-OD_2 group resonance is located between the D_3O^+ ion and the Fe_2−OD group.

motion giving rise to the distinct smaller sideband manifolds at 67 K.

The weaker Fe−OD_2 resonance is hidden beneath the more intense D_3O^+ resonance, which prevents a ready determination of its isotropic peak position. Furthermore, between 73 and 69 K the intensity of the Fe−OD_2 group is reduced noticeably and only the broad manifold of ssbs from the D_3O^+ ions are visible. Thus, the plot in Figure 5d only shows the isotropic shift as a function of temperature for the Fe_2−OD and D_3O^+ groups.

■ ANALYSIS OF THE HYPERFINE SHIFT, δ, IN THE PARAMAGNETIC REGIME

A more detailed investigation of the temperature dependence of the hyperfine shift is now performed to investigate the local magnetic couplings further. The interaction between the ^{2}H nuclei and the unpaired electron spins is given by the hyperfine interaction:

$$H_i = A_i S_{z,i} \tag{5}$$

In the paramagnetic regime (>150 K for jarosite), where the electron spin relaxes fast on the NMR time scale, the Hamiltonian can be simplified to the following

$$H_i = A_a \langle S_Z \rangle \tag{6}$$

where $\langle S_Z \rangle$, the time averaged electron spin is given by

$$\langle S_Z \rangle = -\frac{B_0}{\mu_0 g N_A \mu_B} \chi_M \tag{7}$$

and B_0 is the static magnetic field, μ_0 the permeability, g the electron g factor, N_A Avogadro's number, and μ_B the Bohr magneton. In the Curie−Weiss regime, the isotropic hyperfine shift for a paramagnet is thus similarly expected to follow the CW law

$$\chi = \frac{C}{T - \theta} \tag{8}$$

where C is the Curie constant, T temperature (K), and Θ the Weiss constant above the Néel temperature. If the local spins are not correlated a zero value of Θ is observed. If the correlations are either ferromagnetic or anti ferromagnetic, then either $\Theta > 0$ or $\Theta < 0$, are observed, respectively. Using this, we expect the following relationship between the inverse shift and temperature.

$$\delta(T)^{-1} \propto \frac{T}{C} - \frac{\theta}{C} \tag{9}$$

Thus, we can use the regime in which our ^{2}H NMR data fits the CW law to estimate the Weiss constant (Θ) by interpolating the fit of the data to $\delta(T)^{-1} = 0$, i.e., the intercept with the x-axis; the slope is then given by 1/C. This is illustrated in Figure 10, where the inverse chemical shift is plotted as a function of temperature for all four jarosite samples. For Stoic-jaro, K-jaro, and Na-jaro, only the shifts of the Fe_2−OD groups are plotted and the data are restricted to the Curie−Weiss regime, as summarized in Table 2.

$$\text{stoic-jaro}: \delta(Fe_2\text{−OD})^{-1} = 2.96\times10^{-6}T + 0.0033[\text{ppm}^{-1}] \quad r^2 = 1.00 \tag{10}$$

$$\text{K-jaro}: \delta(Fe_2\text{−OD})^{-1} = 3.36\times10^{-6}T + 0.0033[\text{ppm}^{-1}] \quad r^2 = 0.97 \tag{11}$$

$$\text{Na-jaro}: \delta(Fe_2\text{−OD})^{-1} = 3.37\times10^{-6}T + 0.0036[\text{ppm}^{-1}] \quad r^2 = 0.99 \tag{12}$$

The temperature dependence of $\delta(Fe_2\text{−OD})$ is similar within error-limits for the three samples, the differences between the stoichiometric and defect samples being described to the presence of vacancies in the more distant coordination shells, as discussed above. The Weiss constant (Θ) exhibits some scatter due to the only ca. 40 ppm change in isotropic shift in the examined temperature range and we note that small changes in δ or omission/adding of a data point results in quite large change (300 K) in the Weiss constant. Taking this into consideration, the Θ values for the three samples are similar within error-limits and $\Theta \approx -1000(150)$ K is obtained. This confirms the antiferromagnetic nature of the samples at low temperatures, although our experimentally determined value of Θ is somewhat higher than $\Theta = -812$ to -829 K reported by Grohol et al.[17]

For the D_3O-jaro, the following relation is obtained:

$$D_3O^+: \delta(D_3O)^{-1} = 5.27\times10^{-4}T + 0.036[\text{ppm}^{-1}] \quad r^2 = 0.98 \tag{13}$$

$$Fe_2\text{−OD}: \delta(Fe_2\text{−OD})^{-1} = -6.41\times10^{-6}T + 0.0057[\text{ppm}^{-1}] \quad r^2 = 0.38 \tag{14}$$

The inverse shift (δ) as a function of temperature for the D_3O^+ ion is linear in the entire temperature range, as anticipated for a paramagnet obeying the CW law; however, the fit for the Fe_2−OD group is noticeably poorer.

dx.doi.org/10.1021/cm2003929 |Chem. Mater. 2011, 23, 3176–3187

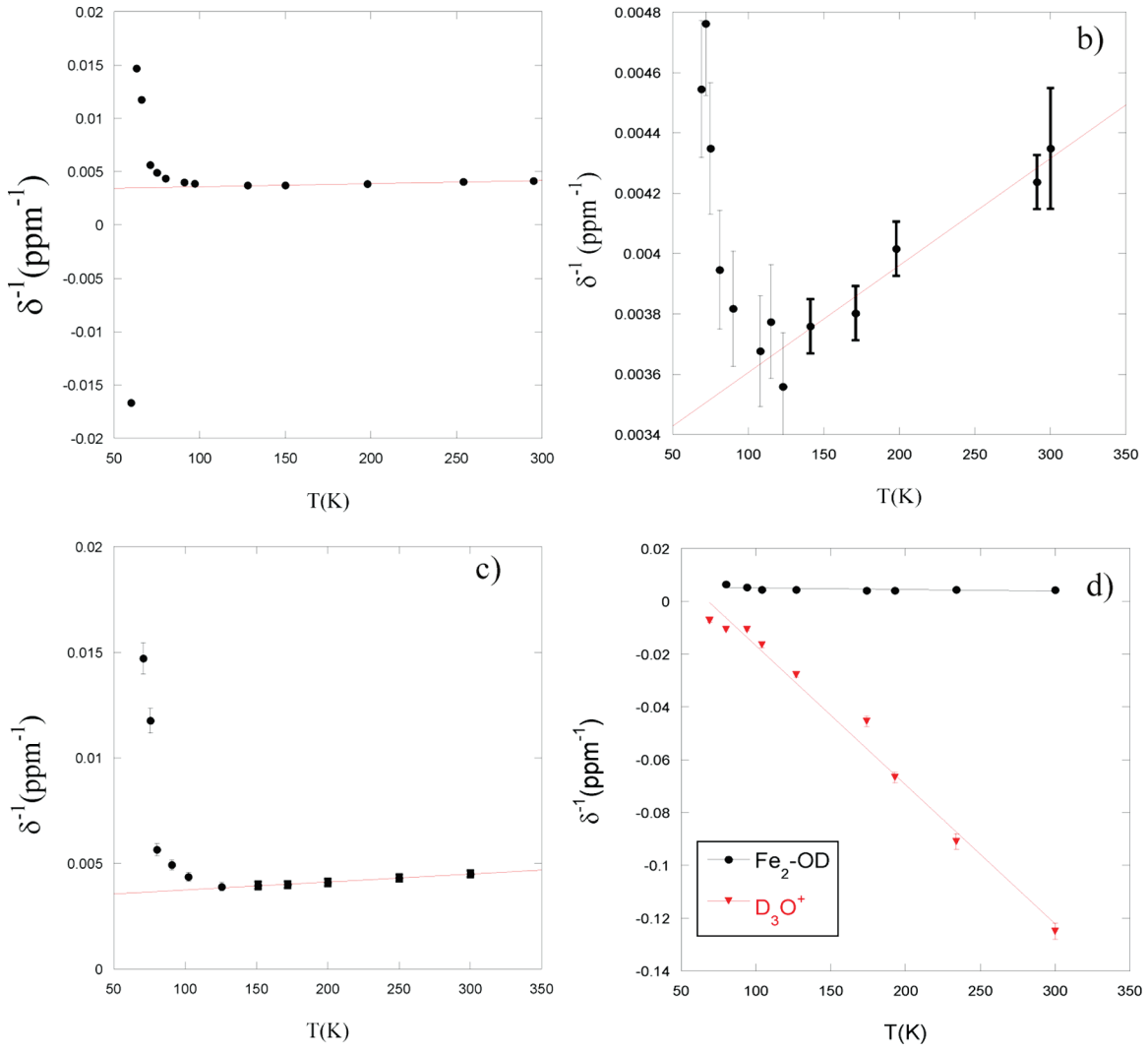

Figure 10. Inverse isotropic (Fe_2OD) shifts as a function of temperature for (a) Stoic-jaro, (b) K-jaro, (c) Na-jaro, and (d) D_3O-jaro (Fe_2OD and D_3O^+) in the Curie−Weiss regime.

This resonance is due to multiple local magnetic environments due to the presence of 5% Fe vacancies, and it has a line width on the order of the total temperature change. In addition, changes in the local hydrogen bonding geometry may also affect the local magnetic interactions. Thus, the average shift may not correctly reflect the temperature dependence of each, but an average of that of all the environments. The D_3O^+ ion, which is present in only in stoichiometric regions of the sample,[23,38] does not experience these effects. Surprisingly, a small (positive) Weiss Constant 68(40) K is observed, as probed by the D_3O^+ ions. Note that the temperature behavior of the shifts for the D_3O^+ ions in Na-jaro is very similar, suggesting that this is an intrinsic property of the jarosite (stoichiometric) framework.

The small (and positive) Weiss constant, which differs from the one measured from magnetic studies (≈ -700 K[26] and -880 K[16]) is tentatively ascribed to the temperature over which the NMR spectra were acquired. Studies by Wills et al. have shown that freezing out of the spins in the spin-glass starts at as high a temperature as 250 K.[36] An additional factor that may influence the temperature dependence of the shifts is the high magnetic fields at which these studies are performed (4.7−8.4 T). High magnetic fields (>1.4 T) disrupt the coupling between the Kagome layers; although the ions in these layers remain antiferromagnetically coupled, the much weaker coupling between the layers becomes ferromagnetic in a high field below the magnetic transition temperature.[15,37] Thus, this may also be an important factor for the spin-glass where the local magnetic ordering occurs over a larger temperature regime.

Finally we note that the deuterons nearby a vacancy in the Fe−OD_2 groups do not obey a CW law in the temperature range studied here, indicating that very strong local antiferromagnetic correlations persist for these groups.

INTERPRETATION OF THE PARAMAGNETIC SHIFTS

Fe(III) in jarosite is located in a slightly distorted octahedral (tetragonal) configuration with distorted tetragonal symmetry.[37] There are four equatorial Fe−O bonds of equal length and two longer axial bonds. The Fe−O−D bond angle is 112° with the D atom located 9° above the Fe−O−Fe plane, pointing toward the apical oxygen on the sulfate group (Figure 1a).[21] The electron configuration for Fe(III) in jarosite is a high-spin $3d^5$. The

dx.doi.org/10.1021/cm2003929 |*Chem. Mater.* 2011, 23, 3176–3187

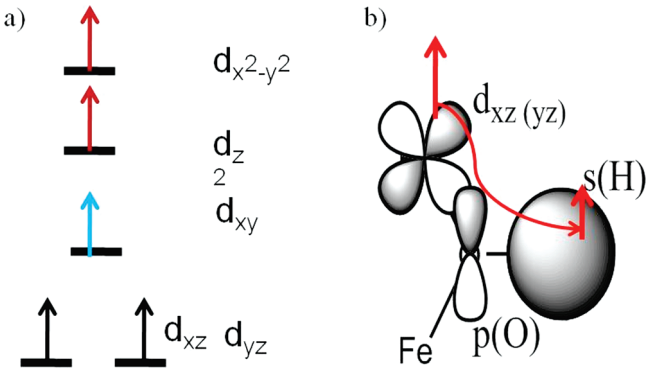

Figure 11. (a) Energy level diagram for Fe(III) d orbitals in jarosite[37] and (b) Delocalization magnetization transfer pathway for jarosite.

distorted coordination environment lifts the degeneracies of the d-electrons so that they are are (from lowest to highest energy): (d_{xz}, d_{yz}), d_{xy}, d_{z^2}, $d_{x^2-y^2}$, as illustrated in Figure 11.[14,37,53]

The hyperfine shift range is usually much larger than the ^{2}H isotropic chemical shift range (ca. 15 ppm), the shift being either positive or negative depending on the d-electron configuration of the transition metal, the local symmetry and bonding environment. The sign of the paramagnetic shifts can be rationalized by using the Goodenough-Kanamori rules.[53] This approach has previously been successfully applied to interpretat of ^{2}H and ^{6,7}Li paramagnetic shifts in iron oxides, jarosite, and manganese oxides and ^{31}P in inorganic cobalt complexes.[50,51,54−60] The predominant contributions to the $\delta(^2H)$ values of Fe_2-OD groups in jarosites arise from transfer through the two Fe(III) bonds via the μ-O atoms. For a half-filled shell, this occurs via a delocalization mechanism (Figure 11b), where unpaired electron spin density is transferred by orbital overlap via the O(2p) orbital to the 1*s* orbital on ^{2}H. The d_{xz} (d_{yz})−p(O)−s(H) transfer pathway has a large overlap and results in a large ferromagnetic (positive) shift in jarosite type structure.[23,53,61] The net effect being a 300(20) ppm shift at $T = 0$.

Fairly small paramagnetic shifts (<200 ppm) seem to be common for inorganic iron compounds including the two iron-(III) oxyhydroxide polymorphs goethite (α-FeOOH) and lepidocrocite (β-FeOOH). The reduction in shift in part arises from the residual antiferromagnetic interactions above $T_{Néel}$,[49] as evident by the weak temperature dependence of $\delta(^2H)$ for the Fe_2-OD group in the temperature range investigated (Figure 5).[48,50,51,62,63] For the Fe-OD_2 group, a shift half (115 ppm) that of the Fe_2-OD group is expected. However, the observed paramagnetic shift is smaller (70 ppm), which is ascribed to small changes in bond angle and an elongation of the O−D bond, as discussed in detail in ref 23.

■ ORIGIN OF SPIN-GLASS BEHAVIOR IN HYDRONIUM JAROSITE

It remains an ongoing discussion as to why hydronium jarosite is a spin-glass: (1) Wills and Harrison originally ascribed this to the presence of defects and local disorder of the hydronium ion,[26,34] (2) Nocera et al. then suggested that an acid−base reaction (eq 1) creates structural disorder,[17] and (3) Bisson and Wills more recently proposed that the spin glass behavior is closely related to the distortion of the FeO_6 octahedron (which in hydronium jarosite is significantly smaller than in other jarosites) and not to disorder as earlier proposed.[29] Our ^{2}H NMR results show that the A^+ site is predominantly occupied by D_3O^+ and no signs of chemical exchange (to form Fe−O-(D_2)−Fe are observed in the ^{2}H NMR spectra: distinct Fe_2-OD and D_3O^+ groups are seen clearly until 90 K. Moreover, we recently demonstrated that the H_3O^+ ion remains intact in stoichiometric regions of both stoichiometric hydronium and deuteronium alunite, as well as in the solid-solution $K-H_3O$ alunite, materials whose spectra are not complicated by the presence of paramagnetic ions.[38,64] (Terminal) $Fe-OH_2$ groups are observed but these are correlated with the concentration of structural defects and not D_3O^+ ions. In addition, recent MD simulations of the isostructural hydronium alunite by Gale et al.[65] did not show signs of proton transfer. Thus, a proton transfer reaction (eq 1) does not seem to be a likely explanation for the spin-glass behavior. Hydrogen bonding of the disordered D_3O^+ ions to the framework must, however, serve to communicate the effect of the disorder in cation positions to the framework.

Our ^{2}H NMR results for hydronium jarosite show that the rotation of the D_3O^+ ion slows between 90 and 73 K prior to the Néel temperature in jarosite but there appears to be a distribution of correlation times and/or magnetic interactions. On the basis of prior structural data, H is expected to occupy the 18 h position with an occupancy of 1/2,[36] and thus the protons are structurally disordered. This is in agreement the recent first principles and MD calculations for hydronium alunite[65] that revealed a high degree of disorder and rapid reorientation of the D_3O^+ ion at 298 K. The freezing of the D_3O^+ motion (on the NMR time scale) before the Néel temperature may prevent the ordering of the magnetic spins. The NMR data thus support the disorder theory by Wills and Harrison,[26,34] but do not contradict the FeO_6 distortion theory. Interestingly, the same temperature behavior for the D_3O^+ ions in Na-jaro and hydronium jarosite suggests that either the FeO_6 distortions must be very local in nature, or that indeed D_3O^+ disorder does play an important role. The FeO_6 distortion hypothesis is supported by our observation of a 14% smaller ^{27}Al quadrupole coupling, i.e., a less distorted AlO_6 octahedron, in the isostructural hydronium alunite (C_Q = 8.6 MHz) as compared to alunite and natroalunite (C_Q = 10.2 MHz).[38]

■ CONCLUSIONS

Variable temperature ^{2}H NMR spectroscopy gives detailed insight into the local magnetic properties of stoichiometric and defect jarosite samples. Based on the temperature dependence of the shifts, two different types of local environments can be resolved (i) stoichiometric regions with Fe_2-OD and A^+/D_3O^+ ions, in which the temperature dependence is proportional to the bulk susceptibility and (ii) defect regions, where the temperature has only a small effect on the shifts of the Fe-OD_2 and D_2O groups implying strong local antiferromagnetic interactions. The motion of the D_3O^+ ion on the NMR time scale freezes at 125(10) K, which is accompanied by a relatively sharp minimum in the T_1 for D_3O-alu at ca. 125 K corresponding to E_a = 6.3(4) kJ/mol. This implies a freezing of the motion and consequent structural disorder of the D_3O^+ ion on the various possible cation positions prior to (a possible) antiferromagnetic ordering, thereby promoting the formation of a spin glass. No sign of proton transfer reactions between H_3O^+ and Fe_2-OD (eq 1) are observed for both D_3O-alu and D_3O-jaro over a wide (250 K) temperature range.

dx.doi.org/10.1021/cm2003929 |*Chem. Mater.* 2011, 23, 3176–3187

Our work demonstrates that probing paramagnetic shifts as a function of temperature gives detailed information about the local magnetic environment, and is complementary to susceptibility measurements, which gives the bulk magnetic properties of the samples. Variable temperature NMR can be applied to gain insight into the local magnetic properties, which is of importance in studies of a variety of paramagnetic materials including soil minerals, catalysts, battery materials and bioinorganic metalorganic complexes, where the presence of paramagnetic transition metal ions is key for their function and properties.

AUTHOR INFORMATION

Corresponding Author

*Fax: +45 6615 8780 (U.G.N.). E-mail: ugn@ifk.sdu.dk (U.G.N.); cpg27@cam.ac.uk (C.P.G.).

ACKNOWLEDGMENT

U.G.N. acknowledges the "Camille and Henry Dreyfus Postdoctoral Program in Environmental Chemistry", The Danish National Research Council (Steno Fellowship, ANS-272-06-0058), and "The Danish L'Oréal-UNESCO for Women in Science Fellowship" for financial support. C.P.G. and U.G.N. thank the Center for Environmental Molecular Science, supported by the NSF (CHE-0221934), and a collaborative grant in chemistry (CHE-0714183) for funding. I.H. has been supported by Estonian Science Foundation (ETF 8198). Mr. Eno Joon is thanked for assistance with low-temperature NMR equipment.

REFERENCES

(1) Stoffregen, R. E.; Alpers, C. N.; Jambor, J. L. In *Sulfate Minerals—Crystallography, Geochemistry, and Environmental Significance*; Alpers, C. N., Jambor, J. L.Nordstrom, D. K., Eds.; Reviews in Mineralogy & Geochemistry; Mineralogical Society of America: Chantilly, VA, 2000; Vol. 40, pp 453—479.

(2) Harrison, W. T. A. *Curr. Opin. Solid State Mater. Sci.* **2002**, *6*, 407.

(3) Alpers, C. N.; Rye, R. O.; Nordstrom, D. K.; White, L. D.; King, B. S. *Chem. Geol.* **1992**, *96*, 203.

(4) Klingelhöfer, G.; Morris, R. V.; Bernhardt, B.; Schröder, C.; Rodionov, D. S.; de Souza, P. A., Jr.; Yen, A.; Gellert, R.; Evlanov, E. N.; Zubkov, B.; Foh, J.; Bonnes, U.; Kankeleit, E.; Gutlich, P.; Ming, D. W.; Renz, F.; Wdowiak, T.; Squyres, S. W.; Arvidson, R. E. *Science* **2004**, *306*, 1740–1745.

(5) Madden, M. E. E.; Bodnar, R. J.; Rimstidt, J. D. *Nature* **2004**, *431*, 821–823.

(6) Squyres, S. W.; Grotzinger, J. P.; Arvidson, R. E.; Bell, J. F.; Calvin, W.; Christensen, P. R.; Clark, B. C.; Crisp, J. A.; Farrand, W. H.; Herkenhoff, K. E.; Johnson, J. R.; Klingelhöfer, G.; Knoll, A. H.; McLennan, S. M.; McSween, H. Y.; Morris, R. V.; Rice, J. W.; Rieder, R.; Soderblom, L. A. *Science* **2004**, *306*, 1709–1714.

(7) Grohol, D.; Huang, Q.; Toby, B. H.; Lynn, J. W.; Lee, Y. S.; Nocera, D. G. *Phys. Rev. B* **2003**, *68*, 094404.

(8) Grohol, D.; Nocera, D. G. *J. Am. Chem. Soc.* **2002**, *124*, 2640–2646.

(9) Grohol, D.; Papoutsakis, D.; Nocera, D. G. *Angew. Chem., Int. Ed.* **2001**, *40*, 1519.

(10) Townsend, M. G.; Longworth, G.; Roudaut, E. *Phys. Rev. B* **1986**, *33*, 4919.

(11) Greedan, J. E. *J. Mater. Chem.* **2001**, *11*, 37–53.

(12) Elhajal, M.; Canals, B.; Lacroix, C. *Phys. Rev. B* **2002**, *66*, 014422.

(13) Harrison, A. *J.Phys.: Condens. Matter* **2004**, *16*, S553.

(14) Yildirim, T.; Harris, A. B. *Phys. Rev. B* **2006**, *73*, 214446.

(15) Grohol, D.; Matan, K.; Cho, J. H.; Lee, S. H.; Lynn, J. W.; Nocera, D. G.; Lee, Y. S. *Nat. Mater.* **2005**, *4*, 323.

(16) Grohol, D.; Nocera, D. G. *Chem. Mater.* **2007**, *19*, 3061.

(17) Grohol, D.; Nocera, D. G.; Papoutsakis, D. *Phys. Rev. B* **2003**, *67*, 064401.

(18) Harris, A. B.; Kallin, C.; Berlinsky, A. J. *Phys. Rev. B* **1992**, *45*, 2899.

(19) Harrison, A.; Wills, A. S.; Ritter, C. *Physica B* **1998**, *241*, 722.

(20) Inami, T.; Maegawa, S.; Takano, M. *J.Magn. Magn. Mater.* **1998**, *177—181*, 752.

(21) Majzlan, J.; Stevens, R.; Boerio-Goates, J.; Woodfield, B. F.; Navrotsky, A.; Burns, P. C.; Crawford, M. K.; Amos, T. G. *Phys. Chem. Miner.* **2004**, *31*, 518.

(22) Matan, K.; Grohol, D.; Nocera, D. G.; Yildirim, T.; Harris, A. B.; Lee, S. H.; Nagler, S. E.; Lee, Y. S. *Phys. Rev. Lett.* **2006**, *96*, 247201.

(23) Nielsen, U. G.; Majzlan, J.; Grey, C. P. *Chem. Mater.* **2008**, *20*, 2234.

(24) Nishiyama, M.; Maegawa, S.; Inami, T.; Oka, Y. *Phys. Rev. B* **2003**, *67*, 224435.

(25) Wills, A. S.; Harrison, A.; Mentink, S. A. M.; Mason, T. E.; Tun, Z. *Europhys. Lett.* **1998**, *42*, 325.

(26) Wills, A. S.; Harrison, A.; Ritter, C.; Smith, R. I. *Phys. Rev. B* **2000**, *61*, 6156.

(27) Majzlan, J.; Peter, G.; Fisher, R. A.; White, A.; Johnson, M. B.; Woodfield, B.; Boerio-Goates, J. *Phys. Chem. Miner.* **2010**, *37*, 635.

(28) Coomer, F. C.; Harrison, A.; Oakley, G. S.; Kulda, J.; Stewart, J. R.; Stride, J. A.; Fåk, B.; Taylor, J. W.; Visser, D. *J. Phys.: Condend. Mattrt* **2006**, *18*, 8847.

(29) Bisson, W. G.; Wills, A. S. *J. Phys.: Condens. Matter* **2008**, *20*, 5.

(30) de Vries, M. A.; Johal, T. K.; Mirone, A.; Claydon, J. S.; Nilsen, G. J.; Ronnow, H. M.; van der Laan, G.; Harrison, A. *Phys. Rev. B* **2009**, *79*, 9.

(31) Basciano, L. C.; Peterson, R. C. *Am. Mineral.* **2008**, *93*, 853.

(32) Frunzke, J.; Hansen, T.; Harrison, A.; Lord, J. S.; Oakley, G. S.; Visser, D.; Wills, A. S. *J. Mater. Chem.* **2001**, *11*, 179.

(33) Wills, A. S. *Can. J. Phys.* **2001**, *79*, 1501.

(34) Fåk, B.; Coomer, F. C.; Harrison, A.; Visser, D.; Zhitomirsky, M. E. *Epl* **2008**, *81*, 6.

(35) Bartlett, B. M.; Nocera, D. G. *J. Am. Chem. Soc.* **2005**, *127*, 8985.

(36) Wills, A. S.; Harrison, A. *J. Chem. Soc., Faraday Trans.* **1996**, *92*, 2161.

(37) Nocera, D. G.; Bartlett, B. M.; Grohol, D.; Papoutsakis, D.; Shores, M. P. *Chem.—Eur. J.* **2004**, *10*, 3851–3859.

(38) Nielsen, U. G.; Majzlan, J.; Phillips, B. L.; Ziliox, M.; Grey, C. P. *Am. Mineral.* **2007**, *92*, 587.

(39) Ripmeester, J. A.; Ratcliffe, C. I.; Dutrizac, J. E.; Jambor, J. L. *Can. Mineral.* **1986**, *24*, 43.

(40) Massiot, D.; Franck, F.; Mickael, C.; King, I.; Le Calvé, S.; Alonso, B.; Durand, J.-O.; Bujoli, B.; Gan, Z.; Hoatson, G. *Magn. Reson. Chem.* **2002**, *40*, 70.

(41) Carravetta, M.; Danquigny, A.; Mamone, S.; Cuda, F.; Johannessen, O. G.; Heinmaa, I.; Panesar, K.; Stern, R.; Grossel, M. C.; Horsewill, A. J.; Samoson, A.; Murata, M.; Murata, Y.; Komatsu, K.; Levitt, M. H. *Phys. Chem. Chem. Phys.* **2007**, *9*, 4879–4894.

(42) Carravetta, M.; Johannessen, O. G.; Levitt, M. H.; Heinmaa, I.; Stern, R.; Samoson, A.; Horsewill, A. J.; Murata, Y.; Komatsu, K. *J. Chem. Phys.* **2006**, *124*.

(43) Holmes, L.; Peng, L. M.; Heinmaa, I.; O'Dell, L. A.; Smith, M. E.; Vannier, R. N.; Grey, C. P. *Chem. Mater.* **2008**, *20*, 3638.

(44) Torchia, D. A.; Szabo, A. *J. Magn. Reson.* **1982**, *49*, 107.

(45) Spiess, H. W. In *NMR: Basic Principles and Progress*; Springer—Verlag: Berlin, 1978; Vol. 15, p 55.

(46) Slichter, C. P. *Principles of Magnetic Resonance*; Harper & Row: New Yorl, 1963.

(47) Nishiyama, M.; Maegawa, S. *Physica B* **2003**, *329—333*, 1065.

(48) Kim, J.; Middlemiss, D. S.; Chernova, N. A.; Zhu, B. Y. X.; Masquelier, C.; Grey, C. P. *J. Am. Chem. Soc.* **2010**, *132*, 16825.

(49) Soda, G.; Chiba, T. *J. Chem. Phys.* **1969**, *50*, 439.

(50) Cole, K. E.; Paik, Y.; Reeder, R. J.; Schoonen, M.; Grey, C. P. *J. Phys. Chem. B* **2004**, *108*, 6938.
(51) Kim, J.; Nielsen, U. G.; Grey, C. P. *J. Am. Chem. Soc.* **2008**, *130*, 1285.
(52) Jakobsen, H. J.; Bildsøe, H.; Skibsted, J.; Giavani, T. *J. Am. Chem. Soc.* **2001**, *123*, 5098.
(53) Goodenough, J. B. *Magnetism and the Chemical Bonding*; John Wiley & Sons: New York, 1963.
(54) Grey, C. P.; Lee, Y. J. *Solid State Sci.* **2003**, *5*, 883.
(55) Lee, Y. J.; Grey, C. P. *J. Phys. Chem. B* **2002**, *106*, 3576.
(56) Lee, Y. S.; Yoon, C. S.; Sun, Y. K.; Kobayakawa, K.; Sato, Y. *Electrochem. Commun.* **2002**, *4*, 727.
(57) Paik, Y.; Bowden, W.; Richards, T.; Sirotina, R.; Grey, C. P. *J. Electrochem. Soc.* **2004**, *151*, A998.
(58) Paik, Y.; Osegovic, J. P.; Wang, F.; Bowden, W.; Grey, C. P. *J. Am. Chem. Soc.* **2001**, *123*, 9367.
(59) Johansson, F. B.; Bond, A. D.; Nielsen, U. G.; Moubaraki, B.; Murray, K. S.; Berry, K. J.; Larrabee, J. A.; McKenzie, C. J. *Inorg. Chem.* **2008**, *47*, 5079.
(60) Carlier, D.; Menetrier, M.; Grey, C. P.; Delmas, C.; Ceder, G. *Phys. Rev. B* **2003**, *67*, 14.
(61) Grey, C. P.; Dupre, N. *Chem. Rev.* **2004**, *104*, 4493.
(62) Nielsen, U. G.; Paik, Y.; Julmis, K.; Schoonen, M. A. A.; Reeder, R. J.; Grey, C. P. *J. Phys. Chem. B* **2005**, *109*, 18310.
(63) Kim, J.; Grey, C. P. *Chem. Mater.* **2010**, *22*, 5453.
(64) Grube, E. B.Sc. Thesis, University of Southern Denmark, 2009.
(65) Gale, J. D.; Wright, K.; Hudson-Edwards, K. A. *Am. Mineral.* **2010**, *95*, 1109.
(66) Siminovitch, D. J.; Rance, M.; Jeffrey, K. R.; Brown, M. F. *J. Magn. Reson.* **1984**, *58*, 62.